Applied Catalysis B: Environmental 154–155 (2014) 82–92

Contents lists available at ScienceDirect

Applied Catalysis B: Environmental

journal homepage: www.elsevier.com/locate/apcatb

Preparation of Ru/graphene-meso-macroporous SiO_2 composite and their application to the preferential oxidation of CO in H_2-rich gases

T. Niu[a,b], G.L. Liu[a,b], Y. Liu[a,b,*]

[a] Collaborative Innovation Center of Chemical Science and Engineering (Tianjin), Tianjin University, Tianjin 300072, China
[b] Tianjin Key Laboratory of Applied Catalysis Science and Engineering, School of Chemical Engineering, Tianjin University, Tianjin 300072, China

ARTICLE INFO

Article history:
Received 4 December 2013
Received in revised form 23 January 2014
Accepted 3 February 2014
Available online 12 February 2014

Keywords:
Graphene
Meso-macroporous
Preferential oxidation
Ruthenium
Silica

ABSTRACT

Preparation for graphene (GE)-meso-macroporous SiO_2 composite was studied, the composite was used as the support for Ru and the resulted catalyst was applied to the preferential oxidation of CO (CO-PROX) in H_2-rich gases. The composite was characterized by using techniques of SEM, TEM, XRD, TPR, N_2 adsorption/desorption and XPS. In the preparation, polystyrene foam and a tri-block copolymer of P123 were used as the template for the macropores and the mesopores, respectively. In addition to the macro and the meso pores, there are narrow slit-like pores with width of several nanometers between GE and SiO_2. The highly dispersed Ru nanoparticle can be loaded on the surface of GE in the composite by impregnating. Thus prepared Ru/GE-SiO_2 showed very good catalytic performance for CO-PROX, especially exhibited high activity at low temperature. The GE-SiO_2 composite should possess the properties of both meso-macroporous oxides and graphene, and is a kind of new promising material, in which SiO_2 can be replaced by other oxides.

1. Introduction

Proton exchange membrane fuel cell (PEMFC) [1] which acts as a small-scale power generation system has drawn much attention due to its high-energy conversion efficiency and nearly zero emission. The fuel of hydrogen is generally produced from various hydrocarbons via the steam reforming and the water–gas shift (WGS) reactions. Due to limited thermodynamics of those two catalytic reactions, there is a small amount of CO in the H_2-rich gases, which poisons the platinum anode [2]. Among all methods for CO removal, the preferential oxidation (PROX) of CO is considered to be one of the most promising methods, owing to its efficiency, simplicity and low cost [3,4].

So far, reported catalysts for CO-PROX reaction include noble metal catalysts [5,6], Au-based catalysts [7] and base metal oxide catalysts [8]. Among those, Ru based catalysts exhibit outstanding catalytic properties in terms of extended low temperature range. The supports reported for Ru-based catalysts include Al_2O_3 [9], SiO_2 [10], CeO_2 [11], zeolite and carbon nanotubes (CNTs). Ru/CNTs [12] shows very good catalytic performance for CO-PROX in H_2-rich gases. Li et al. [13] found that the confinement of Ru in the channels of CNTs obviously improved the catalytic activity for CO-PROX in the temperature range of 75 °C to 120 °C, which is attributed to the micro-environment of nano-channels. Wang et al. [14] pointed out that Ru/CNTs possessed a significantly large surface area, and had a strong interaction between functional groups and Ru particles, which are the reasons for the high activity at low temperature.

CNT is formed by rolling up graphene (GE) to the shape of tube in nano-size. Hence, Ru/GE should be active for CO-PROX. GE is a two-dimensional sheet made of carbon atoms with SP^2 structure, which is a much attractive new material owing to its very high mechanical strength, excellent thermal and electrical conductivity and high surface area [15]. Theoretic studies of density functional theory (DFT) have predicted that embedding transition metal elements, such as Pt [16] and Au [17], on graphene should be highly active for CO oxidation. As for Au/GE, the high activity is ascribed to the partially occupied d orbital localized in the vicinity of the Fermi level which is resulted from the interaction of Au atom and graphene. Based on the first-principle method analyzing, Lu [17] predicated that the CO oxidation on Au/GE could occur at room temperature. Similarly, Li [18] predicted that the Fe-anchored graphene oxide should exhibit high catalytic activity for low-temperature CO oxidation. However, the experimental results do not agree with the theoretical predicts. Only a few reports can be found regarding the experimental study on GE supported metal catalyst, and we found only two papers on this subject [19,20]. Both of them, Pt–Ni/GE

* Corresponding author at: Tianjin Key Laboratory of Applied Catalysis Science and Engineering, Department of Catalysis Science and Technology, Tianjin University, Tianjin, China. Tel.: +86 022 87401675.
E-mail address: yuanliu@tju.edu.cn (Y. Liu).

http://dx.doi.org/10.1016/j.apcatb.2014.02.002
0926-3373/

and Pd/GE, can catalyze CO oxidation reaction until a temperature of higher than 100 °C which is much higher than the predicted room temperature.

The contradiction of above should be ascribed to the mass transfer limitation. The length/width of a GE sheet is in micron or tens of microns, and its thickness is in nano size. The nano metal particles on a GE sheet are covered by another GE sheet. The size of the nano metal particles is much smaller than the size of GE sheets, and resultantly, the nano metal particles are enveloped and cannot contact the molecules of the reactant gases. Reports on catalyst using GE as the support for liquid reaction are many, which in many cases exhibit much high activity [21]. In this situation, the GE sheets loaded with an active component, such as palladium, are dispersed in the liquid and not covered by another sheet of GE.

It is a critical challenge to overcome the mass transfer limitation of the GE catalysts in gas phase reaction and other applications. A few reports can be found on this subject. Worsley et al. [22] reported the preparation of a graphene aerogel that used covalent carbon cross-links between graphene sheets instead of physical bonds for keeping higher-order three-dimensional architectures. The application of CNTs faces the similar challenge, as Zhang et al. have pointed in Ref. [23], they have explored a method of growing CNT on resin sphere to produce monolithic CNTs directly as millimeter-scale spheres, and the CNTs sphere showed better catalytic performance than that of CNTs powders for the oxidative dehydrogenation of ethylbenzene.

Meso-macroporous oxides are of great interest in recent years [24]. Reports on their preparation and their application as catalysts or catalyst supports are many [25]. The mesopores can provide large surface area, and the macropores are favorable to the mass transfer. For example, Pt-Ni/meso-macroporous alumina shows very good catalytic performance for CO-PROX [26]. Also, micro-meso-macroporous materials are a focus, in which both the macropores and the mesopores can be acted as the mass transferring passages.

In this work, the technique for preparing meso-macroporous oxides was introduced into the preparation of GE-meso-macroporous SiO_2 composite to overcome the problem of the mass transfer limitation in nano metal/GE catalysts. The results support the theoretical prediction on nano metal/GE catalysts stated above. The composites of GE-meso-macroporous oxides should possess the special properties of both GE and the meso-macroporous oxides, which should be a new kind of promising material with extensive impact.

2. Experimental

2.1. Preparation of graphene and the graphene-meso-macroporous SiO_2 composite

As shown in Scheme 1, graphite oxide (GO) was synthesized from oxidation of flake graphite according to the Hummers method [27]. In each experiment, 0.5 g flake graphite powder and 0.5 g $NaNO_3$ were added into 25 ml concentrated H_2SO_4 in the condition of iced bath. Then, 3 g $KMnO_4$ was added gradually under vigorous stirring, and maintained the stirring at 2 °C for 0.5 h. After that, 46 ml deionized water was slowly added into the solution and the mixture was stirred at 40 °C for 4 h. Then, the mixture was stirred at 98 °C for 15 min, and then, 1 ml H_2O_2 (30 wt%) and 140 ml deionized were added and stirred for 40 min. The resultant graphite oxide solution was filtered and washed with deionized water for several times until to pH 7. The obtained GO solution was ultrasonic treated for 30 min. The layers of unexfoliated graphite oxide were separated out by using centrifugation at 3000 rpm for 5 min. After that, the suspension containing GO was centrifuged at 8000 rpm for 10 min, and it was freeze-dried overnight. The obtained suspension with GO (1.25 mg ml^{-1}) was then used for the following preparation of GE/SiO_2 composites.

The polystyrene (PS) foams which used as macroporous template were obtained from polymerization of styrene in highly concentrated water-in-oil (W/O) emulsions, the details were stated in Ref. [28]. The monolithic GE-meso-macroporous SiO_2 composite was prepared by impregnating PS foam with the mixed

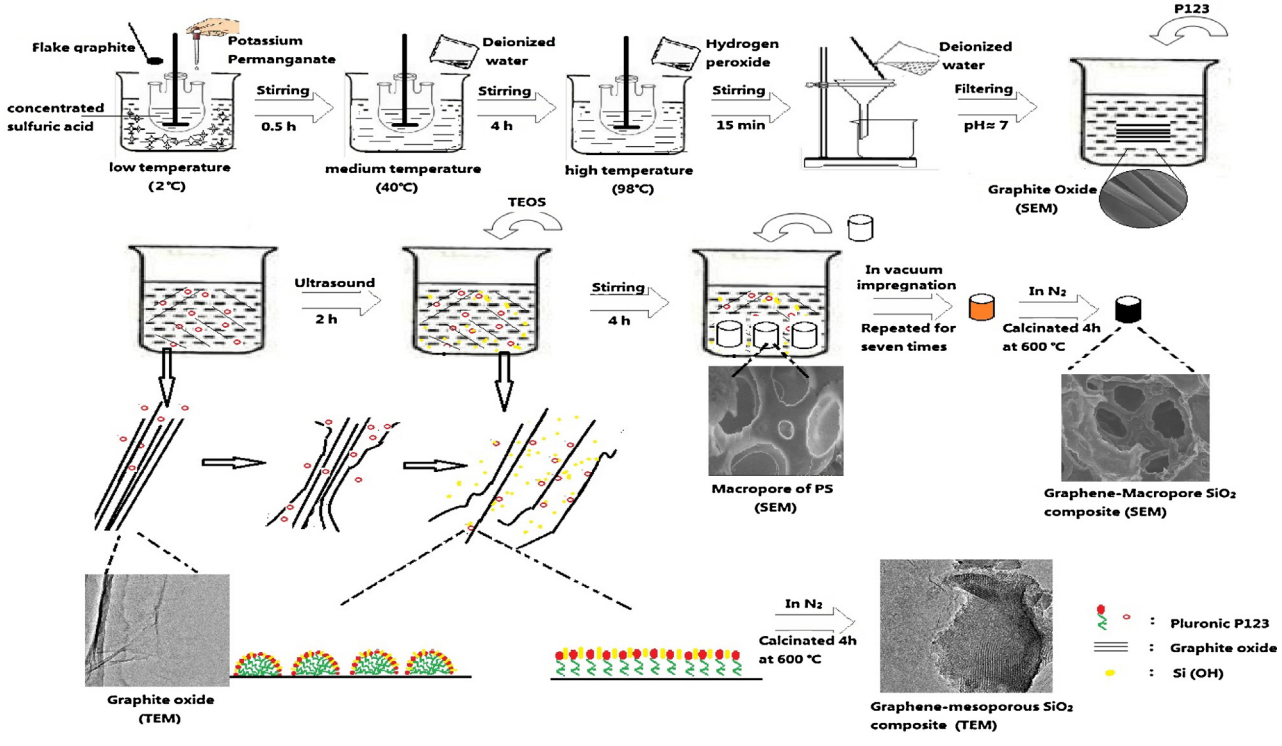

Scheme 1. Catalyst preparation procedures.

sol of silicon oxide hydrosol and GO. At first, P123, a tri-block copolymer (P123) of poly(ethylene oxide)-poly(propylene oxide)-poly(ethylene oxide) was used as the template for the mesopores, was added into the sol solution of GO (1.25 mg/ml), and dispersed by ultrasonic agitation at room temperature for 2 h. Then HCl (2 mol l^{-1}) was dropped into the above suspension, whereafter, was sonicated for 1 h. After that, tetraethyl orthosilicate (TEOS) was added into the above mentioned sol solution at 30 °C and sonicated for 5 h to form silicon hydrosol. At that time, the hydroxyl groups in the TEOS and the P123 bonded with the functional groups (carboxylic acids, epoxy groups and hydroxyl groups) on the GO sheets, as shown in Scheme 1. Then, the PS templates were impregnated into the hydrosol under vacuum condition until no air bubble escaped from the PS template. The impregnated samples were dried at 60 °C for 24 h. This impregnation process was repeated for several times. The dried samples were calcined in N_2 at 600 °C for 4 h to remove P123 and PS template, at the same time the GO could be thermally exfoliated.

2.2. Preparation of Ru/GE-meso-macroporous SiO_2 composite catalysts

The GE-meso-macroporous SiO_2 composite was crushed into 40–60 mesh particles, maintaining the meso-macroporous structure after the crush. The particles of the GE-meso-macroporous SiO_2 were impregnated with a aqueous solution of ruthenium nitrosylnitrate ($Ru(NO)(NO_3)_3{\cdot}xH_2O$). The impregnated samples were freeze-dried overnight. Thus resulted in the monolithic GE-meso-macroporous SiO_2 composite loaded with ruthenium, which was labeled as *x*%Ru/*y*%GE-SiO_2, where *x* and *y* stands for the weight of Ru and graphene in the monolith, respectively. The weight fraction of Ru was defined as

$$\text{Ru wt\%} = \frac{[M]_{Ru}}{[M]_{Ru} + [M]_{SiO_2} + [M]_{GE}}$$

$$\text{GE wt\%} = \frac{[M]_{GE}}{[M]_{SiO_2} + [M]_{GE}}$$

in which $[M]_{Ru}$ is the weight of metal Ru in the catalyst and $[M]_{SiO_2}$ is the weight of SiO_2 support.

$[M]_{GE}$ is the weight of graphene.

2.3. Catalyst characterizations

Nitrogen adsorption and desorption isotherms were measured on a Micromeritics apparatus of model ASAP-2020 at −196 °C. The corresponding specific surface areas were obtained according to the Brunauer–Emmett–Teller (BET) method and the pore size distributions were calculated from the adsorption branch of the isotherm using the Barrett–Jovner–Halenda (BJH) model.

Temperature programmed reduction (TPR) experiments were carried out on a quartz reactor with a reduction gas mixtures of 5 vol% H_2/Ar at a heating rate of 10 °C min^{-1}. 50 mg of sample was loaded in a quartz reactor. Before analysis, the sample was reduced in a gas mixture of 5 vol% H_2/Ar at 300 °C for 2 h and then oxidized in air at 150 °C for 1 h.

Scanning electron microscopy (SEM) characterizations were performed on a Hitachi S4800 field-emission scanning electron microscope with Au-sputtered specimen operated at 15 keV to observe the macroporous structure of the samples.

Transmission electron microscopy (TEM) was performed on a Technai G^2 F20 microscope operated at 200 kV with a high resolution. The samples loaded with ruthenium were pre-treated at 300 °C in a gas mixture of 5 vol% H_2/N_2 for 2 h, then finely grounded in a mortar to fine particles and dispersed by ultrasonication in ethanol. The samples were deposited on aholey Cu gird and dried for measurements.

X-ray photoelectron spectroscopy (XPS) were obtained using Mg *Kα* (*hν* = 1253.6 eV) radiation with PHI-1600 spectrometer (Perkin-Elmer, US). The results were acquired at an X-ray power of 250 W and an energy step of 0.1 eV. Samples were pre-reduced at 300 °C in 5 vol% H_2/N_2 for 2 h. The C1s with binding energy of 284.6 eV was used to correct all XPS spectra.

Catalytic performance tests were carried out on a continuous-flow fixed vertical quartz tube micro-reactor (7.5 mm inner diameter) at atmospheric pressure. First, 100 mg of catalyst was pre-reduced at 300 °C for 2 h in 5 vol% H_2/N_2 at a heating rate of 10 °C min^{-1}. The reaction feed streams comprise of 50 vol% H_2, 1 vol% O_2, 1 vol% CO, and N_2 balance. As for investigating the effect of water and CO_2, 15 vol% H_2O and 12.5 vol% CO_2 was added, respectively. The total flow rate was 40 ml min^{-1}. The reaction temperature was monitored by a thermocouple inserted into the catalyst bed. The effluent gases were analyzed using an on-line gas chromatograph (GC) of SP-3420 equipped with a TCD and a column packed with 5A molecular sieve. FID equipped with a methanator was used to detect CO and CH_4 signals. The CO detection limit was 1 ppm. The activity of catalyst was evaluated by CO conversion, which was defined as followed formula. The selectivity of O_2 for CO oxidation was defined as the ratio of O_2 consumption for the CO oxidation to total O_2 consumption. The formulas were shown as below.

$$\text{Conversion of CO (\%)}: \quad X_{CO} = \frac{[CO]_{in} - [CO]_{out}}{[CO]_{in}} \times 100$$

$$\text{Selectivity of } O_2 \text{ to CO (\%)}: \quad S_{O_2} = \frac{[CO]_{in} - [CO]_{out} - [CH_4]_{out}}{2 \times ([O_2]_{in} - [O_2]_{out})} \times 100$$

$$\text{Yield of } CH_4(\%): Y_{CH_4} = \frac{[CH_4]_{out}}{[CO]_{in}} \times 100$$

$[CO]_{in}$ is the concentration of CO in the feed stream. $[CO]_{out}$ is the concentration of CO in the effluent gases, $[O_2]_{in}$ is the concentration of O_2 in the feed stream. $[O_2]_{out}$ is the concentration of O_2 in the effluent gases. $[CH_4]_{out}$ is the concentration of CO in the feed stream.

3. Results and discussion

3.1. Photographs and SEM images

The morphology of the PS template, graphene and GE/SiO_2 composite are shown by SEM images in Fig. 1. Monolithic GE/SiO_2 composite is successfully prepared by filling PS templates with graphite oxide-silica hydrosols, see Fig. 1(a'). The shape of the GE-SiO_2 monolith (black) was replicated from the PS template (white), except that their size shrank to some degree. The PS templates could be cut into various shapes with a knife, meaning that the GE-SiO_2 monoliths could be in any desired shape.

From image of Fig. 1(a), it can be seen that the macropores of PS template are in a smooth spherical shape mainly ranged from 10 to 40 μm, and interconnected through windows with diameters of several microns, details stated in our previous works [29]. By comparing Fig. 1(a) and (b), it's found that the macroporosity of GE-SiO_2 monolith is the replica of that of the PS template, and such macroporous networks can effectively improve mass transferring.

The appearance of the GE is shown in Fig. 1(c) and (e), and a large wrinkle surface of the GE can be seen clearly from Fig. 1(c). Fasolino et al. [30] pointed out that the spontaneous presence of

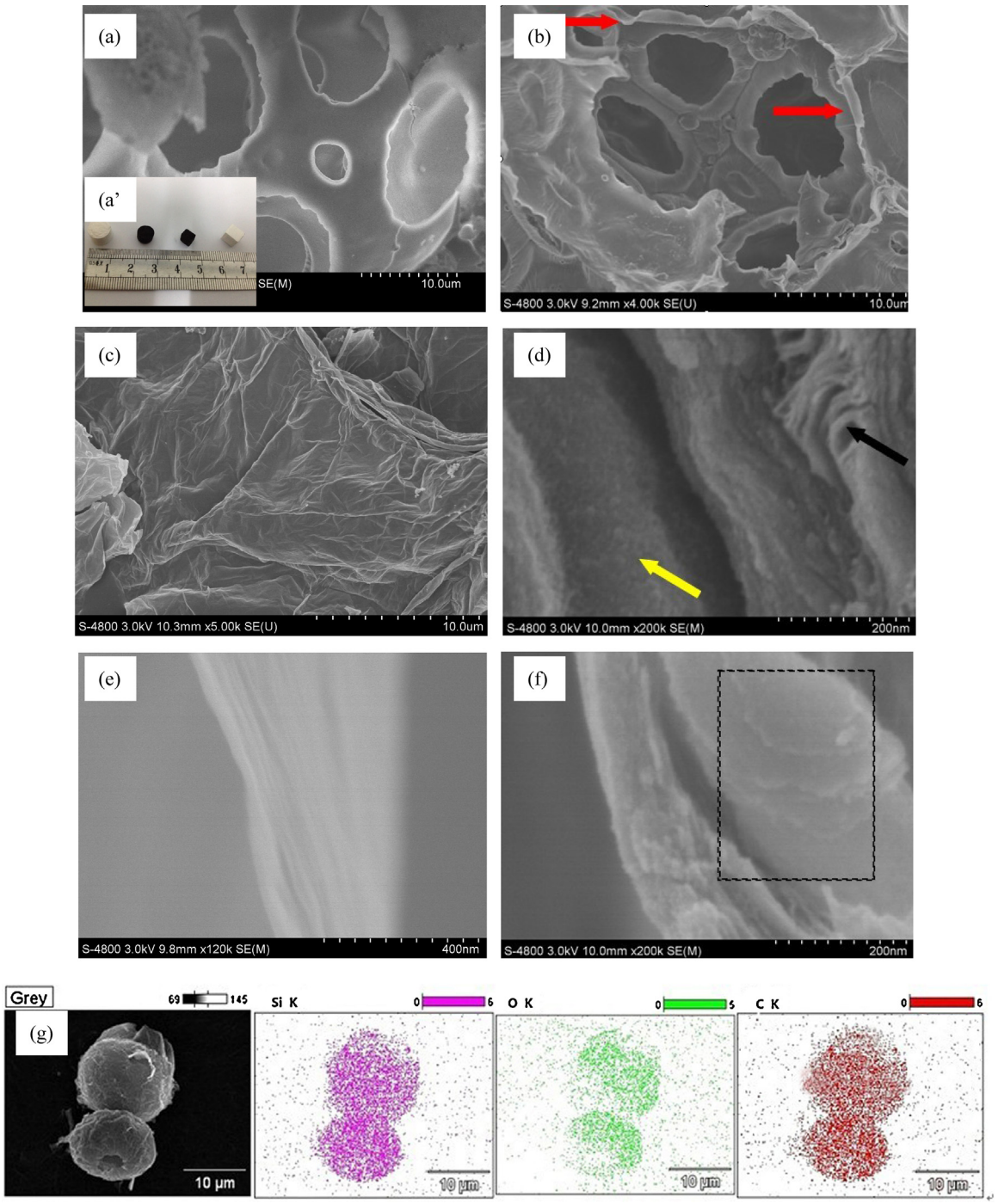

Fig. 1. SEM images of (a) PS temple, (a') photograph of PS and composite, (c, e) graphene and (b, d, f) GE/SiO2 composite with scale bars of (a–c) 10 μm, (e) 400 nm, (d, f) 200 nm, and TEM-EDS images (g) of the composite particles morphologies.

the ripples is owing to thermal fluctuations. The thickness of the thermal exfoliated GO is in the range of around 4–5 nm, as Fig. 1(e) showed.

A part of the GE sheets were covered on the surface of the macropores' walls of SiO_2, as the red arrows directed in Fig. 1(b), and SiO_2 surface exposed in other parts as can be seen in Fig. 1(d). The most of the GE sheets were embedded in amorphous SiO_2 phase, which seems like that GE sheets were inserted into the bulk SiO_2, see the black arrow indicated in Fig. 1(d). There are some slit-like pores with the size of several nano-meters, which should be resulted from the separation of SiO_2 from the surface of the GE sheets in the calcination process. In the calcination process, aggregation of SiO_2 nanoparticles would take place, and the property of SiO_2 is different from GE. The aggregation resulted in the shrinkage of SiO_2 assembly, and thereby the separation of SiO_2 from the GE.

The conformation of the GE-SiO_2 can be seen from another direction. The GE sheets were piled up layer by layer, and between the layers was SiO_2, which could be seen from the dotted box in Fig. 1(f). In the layers between SiO_2 and the GE, there should be some slit-like pores, which could not be seen from this direction. The slit pores are also shown in the following N_2 adsorption–desorption isotherms and TEM results.

The two kinds of the GE, the covering and the inserting, are evenly dispersed in the GE-SiO_2 composite, as SEM-EDS mapping

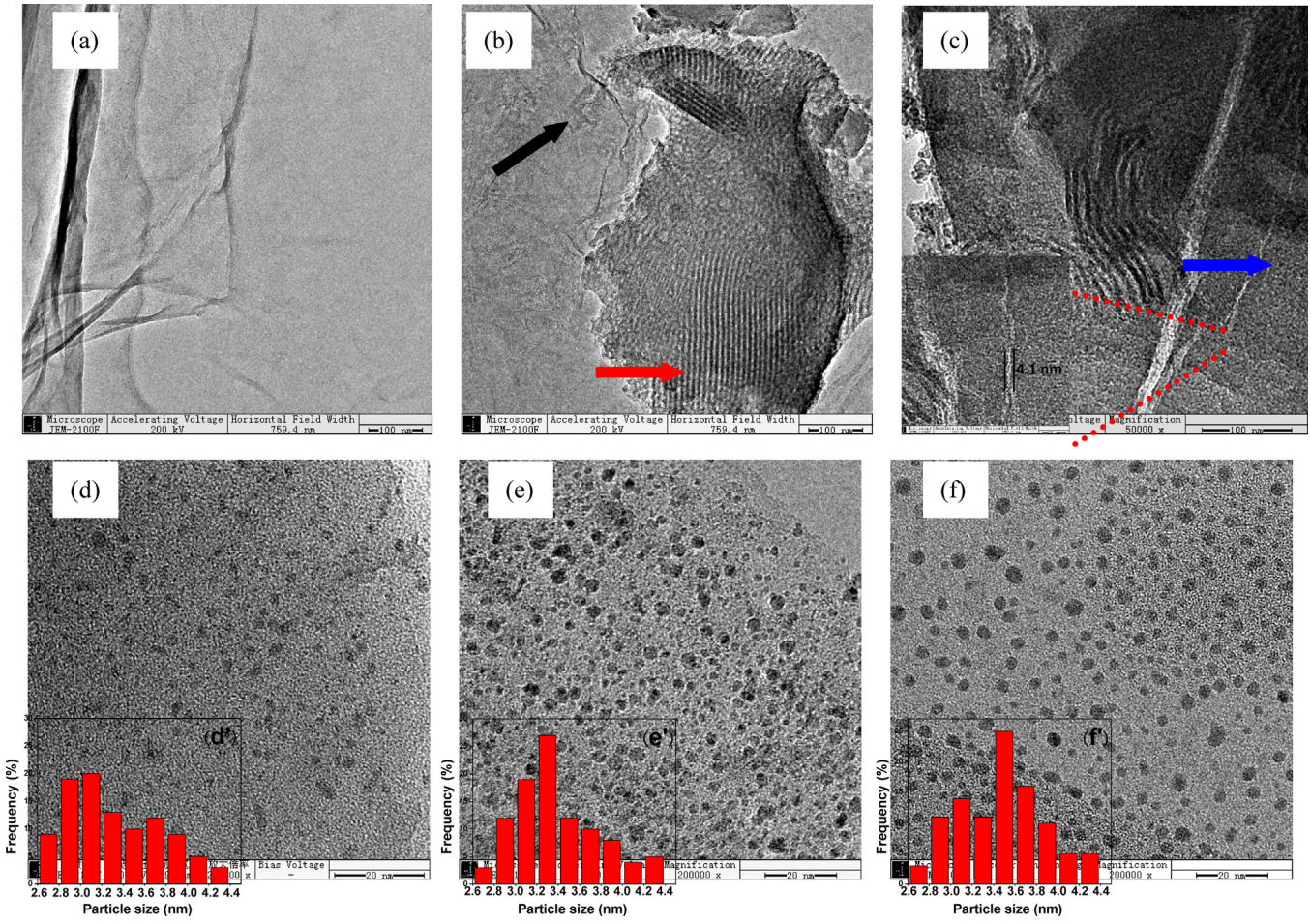

Fig. 2. TEM images of (a) graphene; (b, c) GE-SiO2; (d) 1%Ru-GE/SiO2; (e) 3%Ru-GE/SiO2; (f) 5%Ru-GE/SiO2; Scale bar: 100 nm for (a– c), 20 nm for (d–f). Particle size distributions of Ru in catalyst of (d') 1%Ru-5%GE/SiO2; (e') 3%Ru-5%GE/SiO2; (f') 5%Ru-5%GE/SiO2.

images of Fig. 1(g) show. For a representative part of the composite, silicon (Si K), oxygen (O K) and carbon (C K) can be detected. The Si and C regions are overlapped, and the C layers region match well with the morphology of SiO_2, suggesting that GE and SiO_2 were uniformly mixed.

3.2. Morphology of the catalysts from TEM images

TEM examination characterizations shown in Fig. 2 provide a convenient approach to investigating the morphology of GE, mesoporous SiO_2 and dispersity of Ru nanoparticles. From the images of Fig. 2(b), it is evident that the mesoporous channels in the prepared monolithic silica, which are based on the assisted assembly effect of mesostructure-directing of P123 [31], were parallel, long and highly ordered. The size of unidirectional hexagonal mesoporous structure is around 4 nm, which agrees [32] and in accordance with the results of mesopore size distribution derived from N_2 adsorption listed in Table 1.

From the wrinkle surface in Fig. 2(a), a large GE sheet can be clearly seen, which has little effect on the textural structure of the mesoporosity of SiO_2, as indicated in Fig. 2(b) with the red (representing SiO_2) and black (representing GE) arrows. In other words, the GE-meso-macroporous SiO_2 composite should possess the hierarchical porosity of both the meso-macroporous SiO_2 and the property of GE. The slit-like pores in several nanometers between GE and SiO_2 can also be seen, as indicated by the blue arrows in enlarged Fig. 2(c). The mesopores and the slit-like pores coupled with the macropores (see Fig. 1) may constitute good network for transferring the reactant gas molecules to the surface of the GE.

The morphologies of the loaded Ru nanoparticles on the composite of GE-SiO_2 can be clearly observed from Fig. 2(d–f).The size distributions of Ru nanoparticles are shown in Fig. 2 (d'–f'), which

Table 1
Specific surface area, pore volume and the mesopore size of catalysts derived from N_2 adsorption.

Sample	Specific surface area ($m^2\ g^{-1}$)	Total pore volum ($cm^3\ g^{-1}$)	The most probable pore size (nm)		Average pore diameter (nm)	d_{TEM}[a] (nm)
5%Ru-SiO_2	139	0.107	3.69	–	3.83	2.8
1%GE-SiO_2	231	0.268	3.69	5.59	4.63	
3%GE-SiO_2	289	0.351	3.69	6.60	4.77	3.1
5%GE-SiO_2	347	0.810	3.69	7.67	8.66	3.2
3%Ru/3%GE-SiO_2	285	0.347	3.69	6.57	4.89	
5%Ru/3%GE-SiO_2	280	0.340	3.69	5.55	4.77	

[a] The average sizes of metal Ru particles were statistically analyzed from TEM.

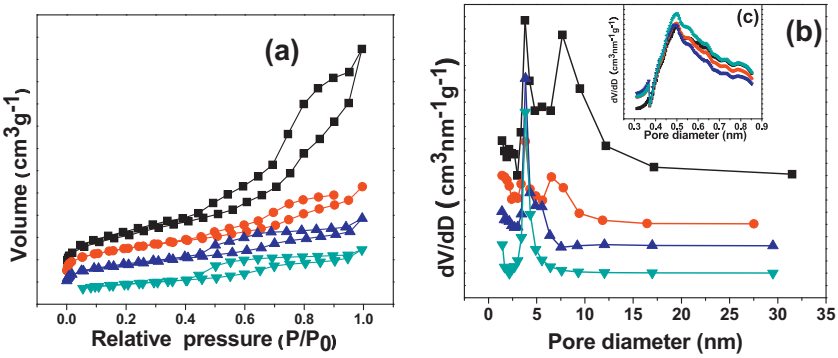

Fig. 3. (a) N2 adsorption–desorption isotherms, (b) BJH mesoporous and (c) micropore size distribution curve of SiO2 (▼), 1%GESiO2(▲), 3%GE-SiO2 (●),5%GE-SiO2 (■).

were obtained by measuring more than 300 particles. The average particle sizes of the Ru particles in the catalysts are 2.9, 3.1 and 3.2 nm for 1%Ru/GE-SiO_2, 3%Ru/GE-SiO_2 and 5%Ru/GE-SiO_2, respectively. The size increased slightly with the increase in the loading amount of ruthenium.

3.3. The results derived from N_2 adsorption–desorption

Nitrogen adsorption–desorption isotherms of the GE-SiO_2 composite and the corresponding BJH pore size distribution are shown in Fig. 3. In all cases, the isotherms are classified as Type IV according to IUPAC definitions [33], which closely related to the properties of mesoporosity. The Type H4 loops at P/P_0 range of 0.65–0.90 present the formation of narrow slit-like pores [34] which should be ascribed to the separation of SiO_2 from the GE sheets as stated above. The loops shift to relatively higher P/P_0 pressure with increasing GE content, suggesting an increase in the size of the mesopores, which may be resulted from the stacking of the GE sheets.

By comparing the pore size distribution profiles of SiO_2 and GE-SiO_2 composite shown in Fig. 3(b), the mesopores with the most probable size of 3.69 nm should belong to the mesopores of SiO_2 assembled from mesostructure-directing template of P123, details of which were stated in [32]. The mesopores at 6.5–10 nm should be the slit-like pores obtained from the separation of SiO_2 and the GE sheets in the calcination process in N_2 at 600 °C.

The addition of GE sheets into the mesoporous SiO_2 has little effect on the microporosity of SiO_2, which can be seen from Fig. 3(c). The microporosity of SiO_2 was formed from the stacking of its fine particles. For the application of silica, it helps to impart a high surface area and pore volume, provides numerous reactive sites, and may be size-selective for molecules [31].

The specific surface area, pore volumes and the most probable mesopore sizes of the composite derived from those isotherms are summarized in Table 1. The specific surface area of the composite increases with increase of the GE content. Especially, the specific surface area of 5%GE- SiO_2 is up to 347 $m^2\ g^{-1}$, which is more than double of the surface area of SiO_2. This should be an indication that the surface of GE sheets was not covered by SiO_2 phase, and there are slit pores between GE and SiO_2, agreeing with above statement. Loading ruthenium led to a little decrease of the specific surface area, pore volume and pore size, which is due to the blockage of some mesopores by the metal Ru particles.

3.4. XRD results

Fig. 4 shows XRD patterns of SiO_2, GO, GE, and GE-SiO_2 catalysts. In Fig. 4(f), the characteristic diffraction peak of graphite oxide (0 0 2) is at $2\theta = 12°$, and the corresponding d-spacing is 7.4 nm between the sheets. This implied that the oxygenated functional groups were generated on both the edges and the sides of the carbon sheets [35]. Those surface functional groups will subsequently act as anchoring sites for the precursor of Ru nanoparticle. The diffraction peak at 43° in Fig. 4(f) is associated with the (1 0 0) plane of the hexagonal structure of carbon. As for XRD patterns of GE from Fig. 3(b), the diffraction peak at 12° completely disappeared. And a broad peak at about 26° with lower intensity was detected, which can be attributed to the ordered crystalline structure of graphene layers. The shifting of GO to higher angle indicate that GO was completely thermal exfoliated [36] in N_2 at 600 °C.

For the XRD patterns of SiO_2, 5%Ru-5%GE/SiO_2 and 5%Ru-3%GE/SiO_2 shown in Fig. 3(a, c, d), little difference could be observed, and the only one broad diffraction peak for each sample is attributed to the amorphous SiO_2 or the overlapping of SiO_2 and GE. No diffraction peaks of ruthenium species could be detected for 5%Ru-5%GE/SiO_2 and 5%Ru-3%GE/SiO_2, suggesting that ruthenium species are highly dispersed, which agrees well with the TEM results of Fig. 2 (f).

For 5%Ru-1%GE/SiO_2 in Fig. 4(e), in which the GE content is at a low level of 1 wt%, a weak diffraction peak corresponding to Ru (1 0 1) at $2\theta = 44.1°$ is observed, and the corresponding size of Ru particle is 6.3 nm derived from the broadness of the peak. It is likely that the such low content of GE can not support the 5 wt% Ru, and resultantly aggregation took place, leading to the larger size of Ru particles. Thus, this should be an indication of that Ru was preferentially loaded on GE rather than on the surface of SiO_2.

3.5. TPR results

The temperature-programmed reduction (TPR) is carried out to probe the reducibility of the oxidized Ru species and interaction

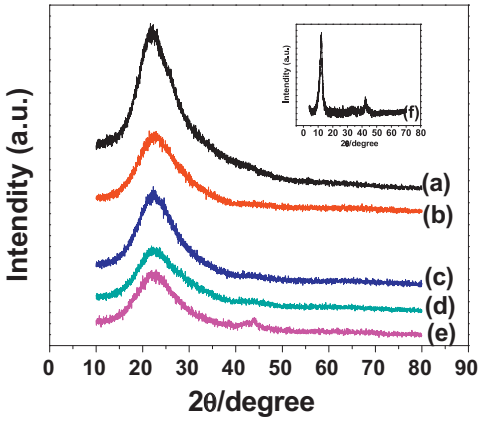

Fig. 4. XRD patterns of (a) SiO2, (b) GE, (c) 5%Ru-5%GE/SiO2, (d) 5%Ru-3%GE/SiO2, (e) 5%Ru-1%GE/SiO2 and(f) GO.

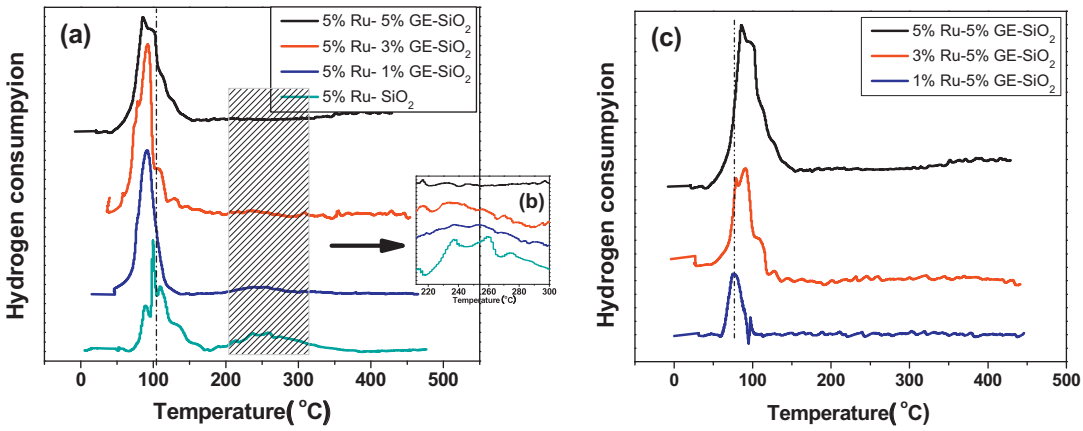

Fig. 5. TPR profiles of (a) 5% Ru supported on GE-SiO2 composite with various GE loading, (b) The enlarged image between 200 °C and 300 °C and (c) various of Ru loaded on the 5%GE-SiO2 composites.

between the ruthenium species and composite support, as showed in Fig. 5(a). For the TPR profile of Ru/SiO_2 catalyst, there are mainly two H_2 consumption peaks, one of which is at T_{max} = 98 °C and the other is at T_{max} = 249 °C. The reduction peak at lower temperature is assigned to the reduction of well-dispersed RuO_x particles interacted with the support. The reduction peaks at the higher temperature correspond to the reduction of crystallized RuO_2 with larger particle size [32].

As for the composite of 5%Ru/1%GE-SiO_2, the reduction peak of the larger RuO_x particle size at 249 °C is obviously weaker than that of 5%Ru/SiO_2 from Fig. 5(a). For Ru/3%GE-SiO_2 and Ru/5%GE-SiO_2, the reduction peak at 249 °C is vanished, which could be seen more clearly from the enlarged profile of Fig. 5(b). This means that the reduction peak at 249 °C is attributed to the reduction of RuO_x on SiO_2 surface. By comparing the H_2 consumption of the peak at 249 °C, it is known that only a small part of Ru was loaded on SiO_2 for 5%Ru/1%GE-SiO_2 due to its low GE content, agreeing with the statement in the above XRD section. For 5%Ru-5%GE/SiO_2 and 5%Ru-3%GE/SiO_2, Ru particles were on the surface of the GE. This suggests that Ru species were absorbed on GE preferentially, compared with that on the surface of SiO_2.

The reduction peak at 88 °C slightly shifts to a lower temperature with increased GE content of the composite catalysts. The reason may be contributed to the larger surface area provided by more GE support, which led to a smaller particle size of metal Ru, for Ru particles are mainly loaded on the GE. It has indicated from the TEM results that the size of Ru particles decreases a little with increasing GE content in the composite.

For the loaded metal oxide particles, the smaller particle size was generally reduced at lower temperature [37], and this statement is supported by the TPR results in Fig. 5(c) for RuO_x supported on GE-SiO_2 composite. RuO_x in 1%Ru/5%GE-SiO_2 exhibits the lowest reduction temperature, and the reduction temperature of RuO_x increases with the increase in the loading amount of Ru, which lead to the increase of the size of Ru particles.

Due to the inevitable functional groups and carbon vacancy defect existed on the surface of graphene, metal ions can be readily adsorbed or embedded on the surface of graphene to form stable metal–graphene composites [38]. Li et al. [20] confirmed that the oxygen-rich groups played an important role in stabilizing Pd clusters and high dispersing on graphene by Raman and XPS characterizations. Zhu et al. [39] prepared well-dispersed Au particles on 2-D graphene oxide and pointed out that the gold nanoparticle can chemically bond with graphene. Compared with pure silica, Hao and coworkers [40] studied the adsorption behavior of SiO_2/graphene composite and found that the composite showed high efficiency and high selectivity toward Pb(II) with the maximum adsorption capacity. The above studies support the statement of that Ru is preferentially loaded on the surface of the GE in the SiO_2-GE composite. In addition to the adsorption sites of the functional groups and the defects on GE, the meso-macropores including the slit-like pores between GE and SiO_2 have provided sufficient passes for the Ru species going to the GE surface.

3.6. The XPS results

In order to further confirm the statement that ruthenium species were preferentially adsorbed on the surface of GE in the GE-SiO_2 composite, XPS spectrum for Ru 3p regions were obtained and shown in Fig. 6. It can be seen that the binding energy of $Ru3p_{1/2}$ for 3%Ru/5%GE-SiO_2 is around 461.1 eV, which is lower than that for 3%Ru/SiO_2 catalyst of around 462.2 eV, indicating that ruthenium in Ru/GE-SiO_2 has lower valence state. The lower binding energy of ruthenium in Ru/GE-SiO_2 is likely attributed to the electron-donating effect of the π electron on the graphene. The carbon atoms in GE are at the state of sp^2 hybrid, and a carbon atom forms three strong σ bonds with other three surrounding atoms. The overlap of the left electrons in p_z orbital on each carbon atoms make up a big π bond, which can donate electrons. Hence, the XPS results support the statement of Ru particles being on the surface of the GE in Ru/GE-SiO_2.

The binding energy spectra can be simulated in association with two different states of ruthenium, Ru metal and RuO_2. The Ru 3p binding energy of 462.4 eV can be ascribed to $Ru^{(0)}$, and that for RuO_2 is at 466.1 eV, as reported by Park [41]. The calculated results are as follows and shown in Fig. 6(c). For 3% Ru/SiO_2, metal Ru in the total ruthenium is 67.1%; and for 3%Ru/GE-SiO_2, the ratio is 80.5%. This means that ruthenium species are in lower valence state in Ru/GE-SiO_2, agreeing with the point view in the above paragraph.

The XPS results suggest that the GE support is favorable for keeping Ru in the state of $Ru^{(0)}$, which is the active site for CO-PROX reaction [42]. It may be predicted that Ru/GE and Ru/GE-SiO_2 are more active for CO oxidation than Ru/SiO_2 is.

For GE-SiO_2 composite used as a catalyst support, if loading one active component on SiO_2 and loading another on GE, a bi-functional catalyst could be produced. This is an interesting application field for GE-SiO_2 composite, or for GE-oxides composites if extended.

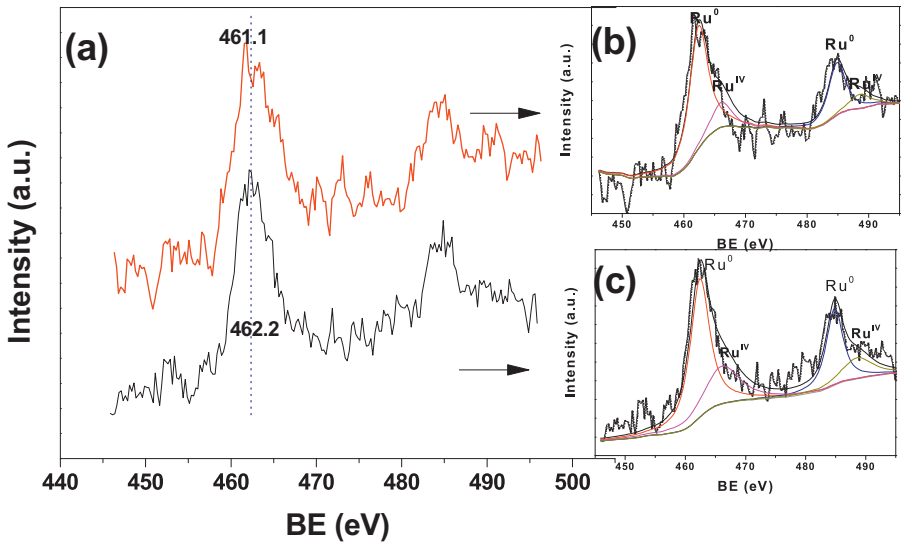

Fig. 6. XPS spectra of (a) Ru 3p for 3%Ru/5%GE-SiO2 (red line) and 3%Ru/SiO2 (black line), and (b, c) corresponding peak simulating. (For interpretation of the references to color in this figure legend, the reader is referred to the web version of this article.)

3.7. *Catalytic performance of Ru/GE-SiO_2*

Fig. 7 illustrates the variations of CO conversion with reaction temperature for CO-PROX over Ru/GE-SiO_2 with Ru contents ranging from 1 to 5 wt%. The CO conversion is dependent on the amount of loaded Ru. The higher the amount of loaded Ru is, the better the low-temperature activity is. 5% GE-5% Ru-SiO_2 in Fig. 7(c) shows the best catalytic performance in all catalysts, that is, CO can be completely purified in the range of 50 to100 °C, and CO could be eliminated to below 21 ppm at 40 °C.

It is worth mentioning that CO conversion increases again with further increase of the reaction temperature at 175 °C or higher, and 100% conversion was achieved at temperatures above 200 °C. This is attributed to the methanation of CO, as shown in Fig. 7(a'–c'). As the reaction temperature was higher than 175 °C, the selectivity of O_2 for CO oxidation decreased, and the selectivity of O_2 for H_2 oxidation increased; while CO could react with H_2 to generate methane and was thus eliminated. Utaka et al. [43] reported the similar methanation reaction over supported Ru catalysts.

Compared with the catalyst of 1%Ru/SiO_2 in Fig. 7(c), Ru/GE-SiO_2 showed much better low-temperature activity. The catalytic activity of Ru/GE-SiO_2 is far higher than those of SiO_2-based catalysts reported in literatures, and it was recognized that SiO_2 is one of the best supports for Ru for CO-PROX [32,44,45]. For example, under the similar reaction conditions, the temperature range for complete elimination of CO over the highly dispersed Ru/SiO_2 is 120–150 °C [44]. Over another highly active catalyst of Pt-Ru/SiO_2, CO could be completely eliminated at the temperature range of 100–140 °C [45]. As stated above, in Ru/GE-SiO_2, the active component of Ru is on the surface of GE. Ru/GE where GE is the support is much more active for CO oxidation than Ru/SiO_2 does.

As stated in Section 1 above, Lu [17] and Li [18] predicted theoretically that noble metal supported on GE should be active at low temperature, while the experimental results reported before did not support this prediction. More specifically, over Pt-Ni/GE catalyst [19] complete conversion of CO was exhibited until 175 °C under the conditions of 1% CO, 20% O_2 and 79 vol% N_2 at a space velocity of 98,000 ml g_{cat}^{-1} h^{-1}. In another case [20], Pd/GE catalyst was tested in the temperature range of 40–160 °C for CO oxidation under the reaction conditions of 1% CO, 20% O_2 and 79 vol% N_2 at a space velocity of 200,000 ml g_{cat}^{-1} h^{-1}. The CO conversion increases gradually with the increasing temperature, and the complete conversion of CO was achieved at 144, 127 and 119 °C, respectively, over the catalysts with 2, 6 and 10 wt% of Pd loading, respectively.

The results of Ru/GE-SiO_2 catalysts in this work support this prediction. Over 5%Ru/5%GE-SiO_2, CO was eliminated to lower than 21 ppm at 40 °C. To note that in Refs. [19,20], the volume fraction of O_2 in the reactant is 20%, which is much higher than 1% for testing Ru/GE-SiO_2 catalysts. The active nanoparticles loaded on GE sheets in the case of Refs. [19,20] tended to be sandwiched between the sheets. Namely, particles with size of about 2 nm were sandwiched between two sheets with size of 10 micron, resultantly, reactant gases were baffled to contact the nanoparticles. As for Ru/GE-SiO_2 of this work, at first, GE sheets were distributed uniformly in the GE-SiO_2 composite. Second, the hierarchically-porosity of Ru/GE-SiO_2 provided very efficient passes for transferring the reactant gases. The meso-macropores and the narrow slit-like pores between GE and SiO_2 constructed a connected and open network for the reactant molecules transmitting.

CO oxidation including CO-PROX is a much rapid reaction, therefore improving mass transferring is important. Thus, catalyst with macroporosity is favorable for CO-PROX, which was studied in our previous works. As in [46], when the macro-pores of CuO–CeO_2 were destroyed, the temperature window for complete purifying CO was narrowed a lot. While, the catalyst of macroporous CuO–CeO_2 can effectively eliminate the CO concentration to below 1 ppm from 150 to 175 °C even at the high space velocity of 160,000 ml g^{-1} h^{-1}. For another case, Pt-Ni/meso-macroporous Al_2O_3 catalyst [26] showed excellent catalytic performance contributed to the macro-pores favoring the mass transfer.

Up to now, the catalytic mechanism over Ru/GE for CO-PROX reaction has not been reported yet. While, mechanism studies on Ru/CNTs can be found. It is reported that CNTs can provide large surface area and have functional groups which can interact with Ru nanoparticles, presenting a better Ru dispersion, which accounts for the superior catalytic activity of Ru/CNT for PROX-CO reaction [14].

The main view points in the theoretical studies on the mechanism for Pt/GE [16], Au/GE [17,47] and FeO_x/GE [18] are as follows. Take Au/GE as the example, Au is in interaction with GE and the interaction affects the adsorption of O_2 on Au. Compare to Au supported on an inert support, Au in Au/GE has stronger electron-donating effect to the adsorbed molecules of O_2. The intensified

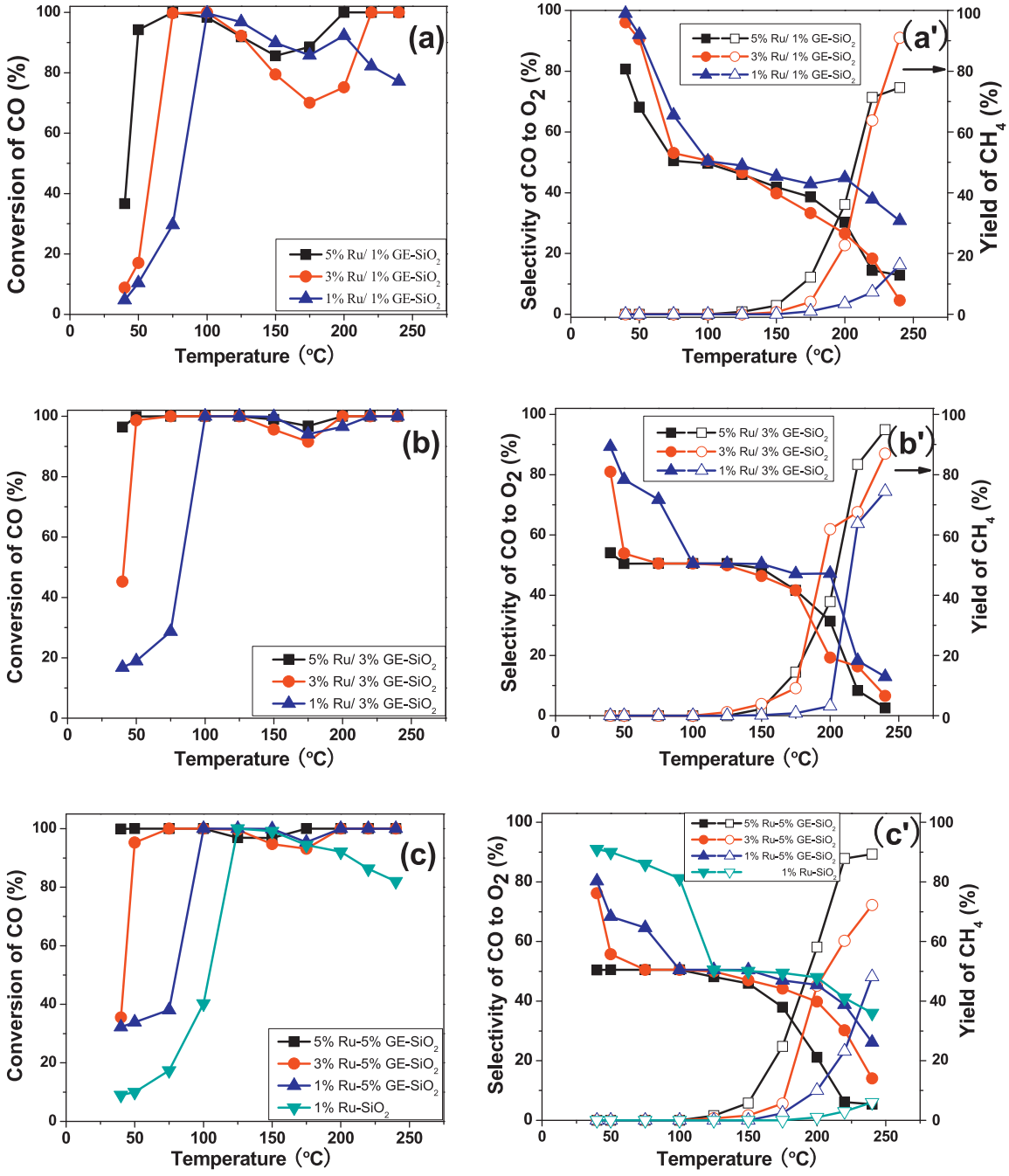

Fig. 7. Variation of CO conversion with reaction temperature (a), the O_2 selectivity to CO oxidation and yield of CH4 (b) for CO-PROX over Ru/GE-SiO_2 catalysts. Reaction conditions: 1 vol% CO, 1 vol% O2, 50 vol% H2 and N2 balance, space velocity = 24,000 ml g_{cat}^{-1} h^{-1}.

electron-donating effect weakens the bond between the two oxygen atoms, as a result, the oxygen is reactive and readily to react with CO to generate CO_2. The XPS results in Fig. 6 indicate that the binding energy of Ru3p in Ru/GE-SiO_2 is lower than that in Ru/SiO_2, meaning that GE support favors Ru donating electron. This agrees with the theoretical studies.

It can be seen that by comparing the results in Fig. 7(a–c), the activity of the Ru/GE-SiO_2 was enhanced with the increase of the GE content. The reasons are listed as follows. Increasing GE content provided more surface area for loading Ru particles, and resultantly the dispersion of Ru increased, improving the catalytic activity. Fig. 7(a'–c') shows that the yield of CH_4 became higher with increasing Ru loading, and adding GE has similar effect. The more GE was added into the composites, the higher the activity for CO methanation is. It seems that both Ru and GE participate in the activation for CO methanation. Detail studies are needed for the mechanism of the reaction.

H_2-rich gases from the reformer effluent generally contain 10–20 vol% CO_2 and 10–20 vol% vapor water. The effects of CO_2 and H_2O on the catalytic performance of Ru/GE-SiO_2 are presented in Fig. 8. Adding both CO_2 and water vapor has a negative effect for CO removal. Even so, the catalyst showed very good catalytic performance, and the residual CO concentration can be eliminated to below 1 ppm in the temperature range of 105–120 °C over 5%Ru/5%GE-SiO_2. Compared with 5%Ru/3%GE-SiO_2, 5%Ru/SiO_2 exhibited the worse performance. Ru supported on GE shows the superior catalytic activity than that supported on SiO_2. The sizes of metal Ru that were statistically analyzed from TEM were

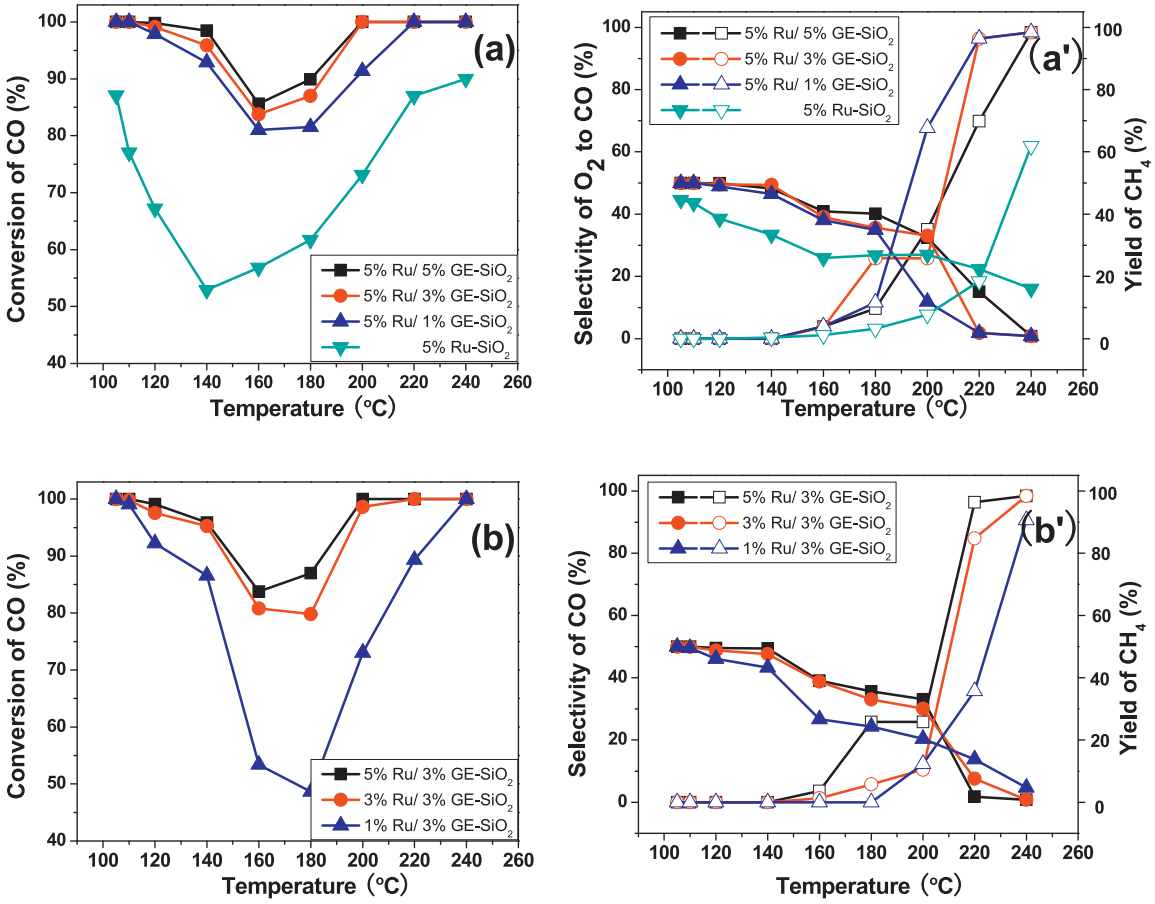

Fig. 8. Variation of CO conversion with reaction temperature (a, b), the O_2 selectivity to CO oxidation and yield of CH_4 (a', b') for CO-PROX over Ru/GE-SiO_2 catalysts. Reaction conditions: 1 vol% CO, 1 vol% O2, 15 vol% H_2O, 12.5 vol% CO_2 and 50 vol% H_2 and N_2 balance, space velocity = 24,000 ml g_{cat}^{-1} h^{-1}.

summarized in Table 1, showing that the average sizes of Ru particles in 5%Ru/SiO_2 and 5%Ru/3%GE-SiO_2 were close, which were 2.8 nm and 3.1 nm, respectively.

The conversion of CO increases with increasing reaction temperature in temperature range of 180 to 240 °C, as can be seen from Fig. 8(a') for Ru/5%GE-SiO_2, which is attributed to the high yield of CH_4. At this temperature range, the selectivity of CO for O_2 was low. Ru/3%GE-SiO_2 catalyst exhibited the similar effects.

Running at T = 105 °C in reaction gases of 1% CO, 1% O_2, 12.5% CO_2, 15% H_2O, 50 vol% H_2 and N_2 balance at a higher space velocity of 48,000 ml g^{-1} h^{-1} was performed to assess the catalyst stability. As for the catalyst of 3%Ru/SiO_2, the running period for complete CO conversion is only 3 h, as can be seen from Fig. 9, and the highest CO conversion dropped to 80.1% during a running period of 36 h. For comparison, 3%Ru/5%GE-SiO_2 shows much better long-term stability during the test of 36 h. Complete CO elimination was maintained for 26 h, after that, the CO conversion slowly decreased to 96% in 36 h of reaction time. The above results of Ru/GE-SiO_2 indicate significant improvement in stability, compared with the catalysts with the similar composition. Ru/CNT could sustain 100% CO conversion and 50% selectivity of O_2 for CO oxidation for 100 h at 373 K in reaction gases of 1.0% CO, 1.0% O_2, 50% H_2 balanced with N_2 [13], in which no water and CO_2 were contained. The presence of water and CO_2 is the main reason for the catalyst deactivation for CO-PROX catalysts [48]. Li et al. [20] had tested the stability of 10% Pd/GE for CO oxidation, and the catalyst was stable at 100 °C for more than 24 h in reaction gases of 1% CO, 20% O_2, and 79 vol% and N_2 balance at a space velocity of 200,000 ml g_{cat}^{-1} h^{-1}, and further prolonging of the reaction time could cause a gradual drop to 90%.

The deactivation of Ru-based catalysts for CO oxidation is generally ascribed to two reasons, that are sintering and oxidation of metal Ru [49]. As for the catalyst of Ru/GE-SiO_2, metal Ru tends to interact with GE as stated above, and the reaction temperature was low. Thus the reason of sintering of metal Ru particles can be exclude. Gao et al. [50] studied Ru/CNT for CO-PROX with co-adding 15% CO_2 and 10% H_2O in the feed stream. CO conversion gradually dropped with reaction time, and attributed the deactivation to the adsorption of CO_2 and water on metal Ru surface which led to the partial oxidation of Ru particles. In the above section of XPS, it is indicated that the GE support is favorable for keeping Ru in the

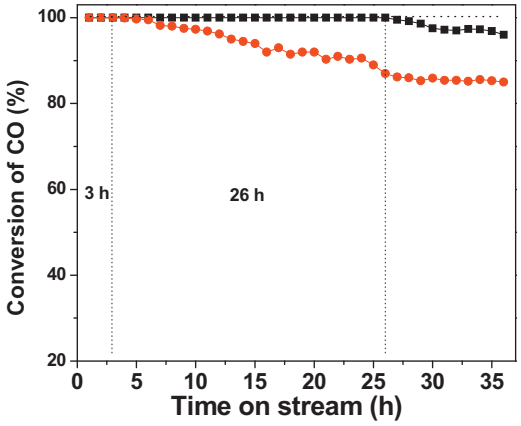

Fig. 9. Endurance tests of 3%Ru-5%GE/SiO2 (■) and 3%Ru/SiO_2 (●). Reaction conditions: 1 vol% CO, 1 vol% O2, 12.5 vol% CO2, 15 vol% H2O, 50 vol% H_2 and N_2 balance at 105 °C and a space velocity of 48,000 ml g_{cat}^{-1} h^{-1}.

state of $Ru^{(0)}$, which is the active site for CO-PROX reaction [42]. Therefore, the surface oxidation of Ru may be the main reason for the catalyst deactivation.

4. Conclusions

The GE-meso-macroporous SiO_2 composite was prepared by filling the mixed sol of graphene and silicon hydrosol into the macroporous polystyrene, and using P123 as the template for the mesopores. The resulted composite has the following characters. SiO_2 and graphene sheets in the composite are uniformly mixed. The macropores have a size range of 10–30 micron and they are connected by windows in several microns. There are mesopores with size of several nano meters in the walls of the macropores which were templated by P123. Narrow slit-like mesopores exist between the graphene sheets and SiO_2.

Ru nanoparticles with high dispersion were selectively loaded on the surface of the graphene sheets of the composite by the simple impregnation method. The resulted Ru/SiO_2-graphene composite showed excellent catalytic activity, high selectivity and good stability for CO-PROX. The meso-macroporosity of the composite provided great porous network for transmitting the reactant gases, which is a main reason for its very good catalytic performance. Ru on graphene tended to be in zero valence state compared with Ru/SiO_2, which may be another reason for its high activity.

Acknowledgments

The financial support of this work by NSFC (No. 21376170, 21263011) and Doctoral Fund of Ministry of Education of China (20100032110019) are gratefully acknowledged.

References

[1] E. Antolini, Appl. Catal., B 123–124 (2012) 52–68.
[2] C. Wang, L. Zhang, Y. Liu, Appl. Catal., B 136–137 (2013) 48–55.
[3] L. Ilieva, T. Tabakova, G. Pantaleo, I. Ivanov, R. Zanella, D. Paneva, N. Velinov, J.W. Sobczak, W. Lisowski, G. Avdeev, A.M. Venezia, Appl. Catal., A 467 (2013) 76–90.
[4] E.D. Park, D. Lee, H.C. Lee, Catal. Today 139 (2009) 280–290.
[5] N. Bion, F. Epron, M. Moreno, F. Mariño, D. Duprez, Top. Catal. 51 (2008) 76–88.
[6] K. Liu, A. Wang, T. Zhang, ASC Catal. 2 (2012) 1165–1178.
[7] T. Shodiya, O. Schmidt, W. Peng, N. Hotz, J. Catal. 300 (2013) 63–69.
[8] G. Avgouropoulos, T. Ioannides, H. Matralis, Appl. Catal., B 56 (2005) 87–93.
[9] S. Lu, Y. Liu, Appl. Catal., B 111–112 (2012) 492–501.
[10] S.-i. Ito, H. Tanaka, Y. Minemura, S. Kameoka, K. Tomishige, K. Kunimori, Appl. Catal., A 273 (2004) 295–302.
[11] X. Liao, W. Chu, X. Dai, V. Pitchon, Appl. Catal., A 449 (2012) 131–138.
[12] R. Nie, D. Liang, L. Shen, J. Gao, P. Chen, Z. Hou, Appl. Catal., B 127 (2012) 212–220.
[13] B. Li, C. Wang, G. Yi, H. Lin, Y. Yuan, Catal. Today 164 (2011) 74–79.
[14] L. Wang, J. Chen, V. Rudolph, Z. Zhu, Adv. Power Technol. 23 (2012) 465–471.
[15] A.K. Geim, Science 324 (2009) 1530–1534.
[16] E.J. Yoo, T. Okata, T. Akita, M. Kohyama, J. Nakamura, I. Honma, Nano Lett. 9 (6) (2009) 2255–2259.
[17] Y.H. Lu, M. Zhou, C. Zhang, Y.P. Feng, J. Phys. Chem. C 113 (47) (2009) 20156–20160.
[18] F. Li, J. Zhao, Z. Chen, J. Phys. Chem. C 116 (2012) 2507–2514.
[19] C. Zhang, W. Lv, Q. Yang, Y. Liu, Appl. Surf. Sci. 258 (2012) 7795–7800.
[20] Y. Li, Y. Yu, J.-G. Wang, J. Song, Q. Li, M. Dong, C.-J. Liu, Appl. Catal., B 125 (2012) 189–196.
[21] T. Truong-Huu, K. Chizari, I. Janowska, M.S. Moldovan, O. Ersen, L.D. Nguyen, M.J. Ledoux, C. Pham-Huu, D. Begin, Catal. Today 189 (2012) 77–82.
[22] M.A. Worsley, T.Y. Olson, J.R.I. Lee, T.M. Willey, M.H. Nielsen, S.K. Roberts, P.J. Pauzauskie, J. Biener, J.H. Satcher, T.F. Baumann, J. Phys. Chem. Lett. 2 (2011) 921–925.
[23] J. Zhang, R. Wang, E. Liu, X. Gao, Z. Sun, F.S. Xiao, F. Girgsdies, D.S. Su, Angew. Chem. Int. Ed. Engl. 51 (2012) 7581–7585.
[24] C.M. Parlett, K. Wilson, A.F. Lee, Chem. Soc. Rev. 42 (2013) 3876–3893.
[25] T. Niu, L.M. Shen, Y. Liu, J. Porous Mater. 20 (2013) 789–798.
[26] S. Lu, Y. Liu, Y. Wang, Chem. Commun. (Camb.) 46 (2010) 634–636.
[27] O.C. Compton, S.T. Nguyen, Small 6 (2010) 711–723.
[28] Y. Zhang, H. Liang, C.Y. Zhao, Y. Liu, J. Mater. Sci. 44 (2008) 931–938.
[29] Y. Zhang, C.Y. Zhao, H. Liang, Y. Liu, Catal. Lett. 127 (2008) 339–347.
[30] A. Fasolino, J.H. Los, M.I. Katsnelson, Nat. Mater. 6 (2007) 858–861.
[31] N.D. Petkovich, A. Stein, Chem. Soc. Rev. 42 (2013) 3721–3739.
[32] T. Niu, C.X. Wang, L.H. Zhang, Y. Liu, Int. J. Hydrogen Energy 38 (2013) 7801–7810.
[33] B. Huang, C.H. Bartholomew, B.F. Woodfield, Microporous Mesoporous Mater. 184 (2014) 112–121.
[34] W.H. Zhang, J.L. Shi, L.Z. Wang, D.S. Yan, Chem. Mater. 12 (5) (2000) 1408–1413.
[35] Y. Zhu, S. Murali, W. Cai, X. Li, J.W. Suk, J.R. Potts, R.S. Ruoff, Adv. Mater. 22 (2010) 3906–3924.
[36] L.Y. Wufeng Chen, P.R. Bangal, J. Phys. Chem. C 114 (2010) 19885–19890.
[37] Y.H. Kim, J.E. Park, H.C. Lee, S.H. Choi, E.D. Park, Appl. Catal., B 127 (2012) 129–136.
[38] I.V. Lightcap, T.H. Kosel, P.V. Kamat, Nano Lett. 10 (2010) 577–583.
[39] C. Zhu, L. Han, P. Hu, S. Dong, Nanoscale 4 (2012) 1641–1646.
[40] L. Hao, H. Song, L. Zhang, X. Wan, Y. Tang, Y. Lv, J. Colloid Interface Sci. 369 (2012) 381–387.
[41] C.B.L.X. Yang, B. MacDougall, J. Park, J. Appl. Electrochem. 34 (2004) 427–438.
[42] M.E.T. Tabata, Catal. Lett. 98 (2004) 37–42.
[43] T. Utaka, T. Okanishi, T. Takeguchi, R. Kikuchi, K. Eguchi, Appl. Catal., A 245 (2003) 343–351.
[44] S.Y. Chin, O.S. Alexeev, M.D. Amiridis, Appl. Catal., A 286 (2) (2005) 157–166.
[45] S. Chin, O. Alexeev, M. Amiridis, J. Catal. 243 (2006) 329–339.
[46] Y. Zhang, H. Liang, X.Y. Gao, Y. Liu, Catal. Commun. 10 (2009) 1432–1436.
[47] M. Zhou, Y.H. Lu, Y.Q. Cai, C. Zhang, Y.P. Feng, Nanotechnology 22 (2011) 385502.
[48] C.M. Bae, J.B. Ko, D.H. Kim, Catal. Commun. 6 (2005) 507–511.
[49] S. Eckle, M. Augustin, H.-G. Anfang, R.J. Behm, Catal. Today 181 (2012) 40–51.
[50] Y. Gao, K. Xie, S. Mi, N. Liu, W. Wang, W. Huang, Int.J.Hydrogen Energy 38 (2013) 16665–16676.